



Die Grenzen der
Chemie neu ausloten?
It takes
#HumanChemistry

Wir suchen kreative Chemikerinnen und Chemiker,
die mit uns gemeinsam neue Wege gehen wollen –
mit Fachwissen, Unternehmertum und Kreativität für
innovative Lösungen. Informieren Sie sich unter:

evonik.de/karriere

3D X-Ray Diffraction Characterization of Grain Growth and Recrystallization in Rolled Braze Clad Aluminum Sheet

Torkel Stenqvist, Johan Hektor, Sara Bylund, Robert Moberg, Mårten O. M. Edwards, Stephen A. Hall,* and Lars-Åke Näslund*

Braze clad on aluminum (Al) sheets has enabled fast and convenient brazing assembly of complex heat exchangers. However, there are details in the brazing process that are not fully understood. Herein, 3D X-ray diffraction (3DXRD) is used to investigate the grain position, size, and orientation before and after controlled atmosphere brazing (CAB). The outcomes are presented as maps of center-of-mass positions with relative grain size distribution and color-coded grain orientations. The results show that, for braze clad Al sheets exposed to CAB simulation, it is possible to distinguish grains from the solidified Al–Si alloy from those in the core Al alloy. It is also possible to distinguish new grains obtained through recrystallization during CAB. Hence, the study shows that stretching of the rolled Al sheet by 6% provides enough stored energy in the core material so that recrystallization occurs during CAB and, in addition, provides conditions for Al–Si alloy grain growth into the core material. While the phenomenon is well known, it is poorly understood for processes in connection with brazing of mechanically formed Al alloy components in heat exchanger assemblies, and these results demonstrate the potential for gaining deeper insights through 3DXRD.

corrosion resistance.^[1,2] The final properties of the heat exchanger are set in the brazing operation, which depends on the brazing cycle used as well as the chosen alloys and their prebrazed states in the production of aluminum. Often the choice of alloy and temper is a trade-off between pre-braze forming of the component, how well the brazing is, and the required fatigue strength of the unit.^[3] Figure 1 shows examples of typical braze clad Al sheet structures in a heat exchanger. The braze clad is in most cases an aluminum–silicon (Al–Si) alloy with a solidus of 577 °C. During brazing at about 600 °C in nitrogen gas, referred to as controlled atmosphere brazing (CAB), the Al–Si braze alloy in the clad layer liquefies and flows to narrow spaces between different exchanger parts by the capillary forces. Upon solidification, the Al–Si alloy will form fillets that join two parts in a heat exchanger assembly, e.g., a fin to a tube, as

1. Introduction

The advantage of using braze clad on aluminum (Al) sheets is that it enables fast and convenient brazing assembly of complex heat exchangers that can meet the tough working requirements in terms of heat performance, strength, formability, and

shown in Figure 1b,c. The brazing performance depends to a large extent on good fillet formation, the effect of the molten braze clad on the core material, and the structural integrity during brazing at temperatures close to the solidus of the material.^[3]

There are many parameters involved in optimizing brazed aluminum sheets, of which one is the grain structure at the interface

T. Stenqvist, S. Bylund, Dr. L.-Å. Näslund
Gränges Sweden AB
Finspång SE-612 81, Sweden
E-mail: lars-ake.naslund@liu.se

T. Stenqvist, Dr. L.-Å. Näslund
Department of Physics, Chemistry and Biology (IFM)
Linköping University
Linköping SE-581 83, Sweden

Dr. J. Hektor
Deutsches Elektronen-Synchrotron (DESY)
Notkestrasse 85, Hamburg 22607, Germany


Dr. J. Hektor
Helmholtz-Zentrum Geesthacht
Notkestrasse 85, Hamburg 22607, Germany

Dr. J. Hektor
LUNARC – Centre for Scientific and Technical Computing at Lund
University
Lund University
Lund SE-221 00, Sweden

Dr. R. Moberg, Dr. M. O. M. Edwards
Uppsala Synchrotron AB
Dag Hammarskjölds väg 34A, Uppsala Science Park, Uppsala SE-75183, Sweden

Dr. S. A. Hall
Division of Solid Mechanics
Lund University
Lund, Sweden
E-mail: stephen.hall@solid.lth.se

Dr. S. A. Hall
Lund Institute of Advanced Neutron and X-Ray Science
Lund SE-221 00, Sweden

 The ORCID identification number(s) for the author(s) of this article can be found under <https://doi.org/10.1002/adem.202100126>.

© 2021 The Authors. Advanced Engineering Materials published by Wiley-VCH GmbH. This is an open access article under the terms of the Creative Commons Attribution License, which permits use, distribution and reproduction in any medium, provided the original work is properly cited.

DOI: 10.1002/adem.202100126

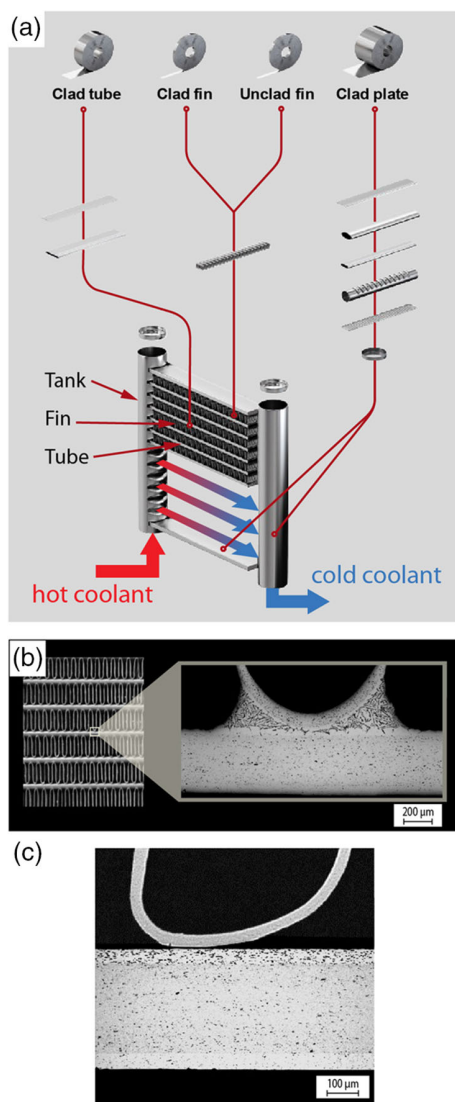


Figure 1. a) A liquid-to-air heat exchanger consists of several parts joined through brazing. The arrows indicate that hot fluid is collected in one tank, pushed through the thin tubes, and cooled as heat is transferred to the fins, which in turn are cooled by the surrounding (forced) air. The cooled fluid is collected in the opposite tank and pushed out in the external circuit that prevents hot parts to become over-heated. b) A cross-section image of a joint between a tube and a fin in a heat exchanger. Molten Al–Si braze clad alloy has flown to the narrow space between the tube and fin materials and formed a joint upon solidification. c) A cross-section image of a fin on top of a tube in a heat exchanger assembly before brazing. The microstructure image shows the Al–Si braze clad alloy on the outside and a corrosion inhibiting Al–Zn alloy on the inside (waterside) of the grayer-core Al alloy tube material. The core Al alloy appears in (b) and (c) as grayer, compared with the Al–Si alloy and the Al–Zn alloy, because of a homogenous distribution of dispersoids.

between the resolidified Al–Si alloy and the core Al material after brazing. The grain structure of the core material is influenced by the chemical composition of the alloy and the thermomechanical processes before brazing but also by the brazing process.^[4–7] In general, the least interaction occurs when the core material has

been fully recrystallized and thus contains of large grains prior to the melting of the braze clad. However, an annealed material with a slight deformation is sensitive for filler attacks, i.e., a process where the liquefied braze clad alters the core material, particularly when the deformation is within the range of 3–10%,^[8] a subject thoroughly presented in a treatise by Wittebrood.^[9]

Information about grain structure has previously been obtained through destructive and time-consuming laboratory techniques such as light optical microscopy (LOM), scanning electron microscopy (SEM), and electron backscatter diffraction (EBSD), which are limited to 2D imaging studies.^[10,11] However, the development of third-generation synchrotron radiation sources has opened up avenues for nondestructive 3D characterization of the microstructure of polycrystalline materials through, e.g., 3D X-ray diffraction (3DXRD).^[12] The Swedish Materials Science beamline (SMS P21) at PETRA III is a hard X-ray beamline mainly designed for wide- and small-angle X-ray scattering (WAXS and SAXS). Through a series of diffraction images, acquired while the sample is being rotated, it is possible to record reflections from all the grains in a polycrystalline sample and assign the diffraction spots with intensities above the signal-to-noise threshold to individual grains from which, e.g., center-of-mass position, unit cell, and grain orientation can be determined. Consequently, the 3D arrangement of the grains in the probed material, including their orientation, can be visualized.^[13] 3DXRD has previously been used successfully in studies of recrystallization and grain growth of pure Al, Al–Mn alloys, and Al–Si alloys, including crystallization kinetics during the liquid-to-solid phase transformation.^[14–18] The aim of the present study was to use 3DXRD to gain further information about the spatial organization, relative size, and orientation of grains at the interface between the Al–Si alloy and the core Al material in a braze-simulated rolled braze clad Al sheet exposed to a sheet forming process prior brazing.

2. Results and Discussions

Figure 2a shows three cross-section LOM images, where the image contrast arises from the interaction of plane-polarized light with individual grains of the rolled Al sheet that was studied in the present work. The sample was 0.15 mm thick and consisted of a 128 µm-thick Al core alloy (core material) and an 18 µm-thick Al–Si clad alloy (braze clad) on one side. The grain size in the core material was 200–800 µm in the rolling direction (RD) and 30–130 µm in the normal direction (ND), i.e., the grains in the core material are elongated along RD. The cross-section images in Figure 2 do not show the grain size in the transverse direction (TD), although grain widths of several hundreds of µm are expected. Hence, the largest grains are estimated to be as big as 800 µm (RD) × 500 µm (TD) × 130 µm (ND). The grain size in the braze clad was, on the contrary, about 10 µm in both RD and ND, as shown in Figure 2b,c. In addition there are a few minute grains in the core material embedded in the large grains. It is suggested that these can grow during subsequent heat treatment if the material is deformed.^[19]

Figure 3a shows a coupon from the sample after it had been exposed to a CAB simulation in nitrogen gas at 590 °C. Both ends of the coupon were in contact with cooling blocks during the

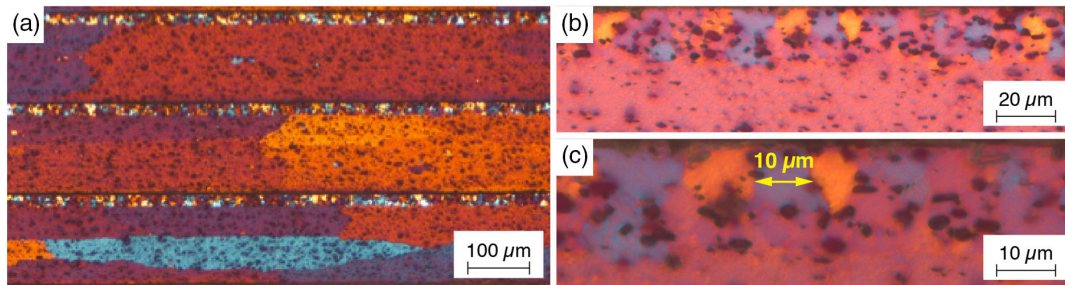


Figure 2. Cross-section-polarized LOM images showing the grain structure for a nontreated sample, i.e., before stretching and braze simulation. Each grain is highlighted by a color, where different colors indicate contrasting crystal orientations of the grains. a) Three layers of the nontreated sample showing large grains in the core material and small grains in the braze clad. There are also a few minute grains in the core material, e.g., in the topmost layer, where there are yellow/blue dots in the large grains colored as purple/brown fields. b) The small grains in the braze clad at a higher magnification (500 \times). c) An estimation of the average grain size indicates 10 μm in diameter along the RD.

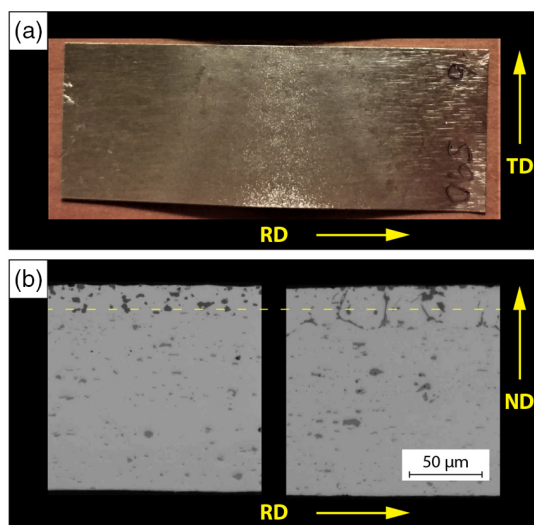


Figure 3. LOM images. a) A coupon exposed to a CAB simulation where both ends have been in contact with cooling blocks and therefore only the center region was “brazed.” The RD is along the long edge and the TD along the short edge. b) Cross-section images of the coupon shown in (a) obtained from one of the non-“brazed” zone (left) and the “brazed” zone (right). The cross section is in the plane defined by the RD and the ND. The Al core material is affected by the braze clad after braze simulation as large Al–Si grains, about 30 μm in diameter, are formed in the intersection; the yellow dashed line highlights the original interface between the core Al alloy and the Al–Si braze clad alloy.

CAB simulation, which kept the ends at a temperature below the melting point of the Al–Si clad alloy, whereas the center part of the coupon has a “brazed” zone, i.e., where the braze clad has been liquefied during braze simulation. Hence, the studied coupon had a non-“brazed” zone, a fully “brazed” zone, and a transition region between them. Figure 3b shows two cross-section LOM images, where the contrast between the Al alloy and hard particles is enhanced through differential interference and where the hard particles appear as dark gray speckles on a light gray background. The left image shows one of the cooled ends of the coupon in Figure 3a, where the interface between the Al–Si clad alloy and the core Al alloy is indicated by the yellow dashed line. The microstructure in the braze clad alloy includes

Si particles (dark gray) between the small Al–Si grains (light gray). The core material, below the dashed line, has a grayer appearance compared with the braze clad because of a homogeneous distribution of dispersoids, mainly, AlMn particles, within the grains. In addition there is a distribution of Al(Fe,Mn)Si constituent particles (dark gray) in the core material. Although the sample was heat treated to a temperature just below the melting point of the Al–Si clad alloy, the interface between the braze clad and the core material is intact. The right image in Figure 3b shows a LOM section through the “brazed” zone of the coupon in Figure 3a, i.e., in the region where the temperature is above the melting point of the Al–Si clad alloy. Large Al–Si grains, decorated by Si particles (dark gray), were formed during the solidification of the molten braze clad and have grown into the core material. The core material has, thus, been attacked by the molten braze clad alloy, which has likely weakened important properties such as strength and corrosion resistance. It is important to note that the material was stretched by 6% prior to the CAB simulation to simulate a sheet-forming process of heat exchanger components before brazing, which can provoke the phenomenon of braze clad alloy penetration into the core material.^[8]

Figure 4 shows the grain structure in the non-“brazed” zone, in the fully “brazed” zone, and in the transition region between them. The RD is along the long edge of the coupon, which made the grains elongate in the direction from the non-“brazed” zone to the fully “brazed” zone in the cross-section images, as shown in Figure 4. The cross-section images show that the non-“brazed” zone has a braze clad that consists of small grains ($\approx 10 \mu\text{m}$), whereas the “brazed” zone has significantly larger grains grown from molten Al–Si alloy ($\approx 30 \mu\text{m}$). Consequently, the interface between the solidified Al–Si grains and the core material has become uneven because the Al–Si grains have grown into the core material. In addition, in the core material, new small grains appear in the “brazed” zone, as shown in Figure 4b,c by white arrows, which are significantly larger than the minute grains that normally are present, highlighted by black arrows. Some of the minute grains in the core material might be new grains, although some might have been present since before the braze simulation, as shown in the core material of the nontreated sample in Figure 2a.

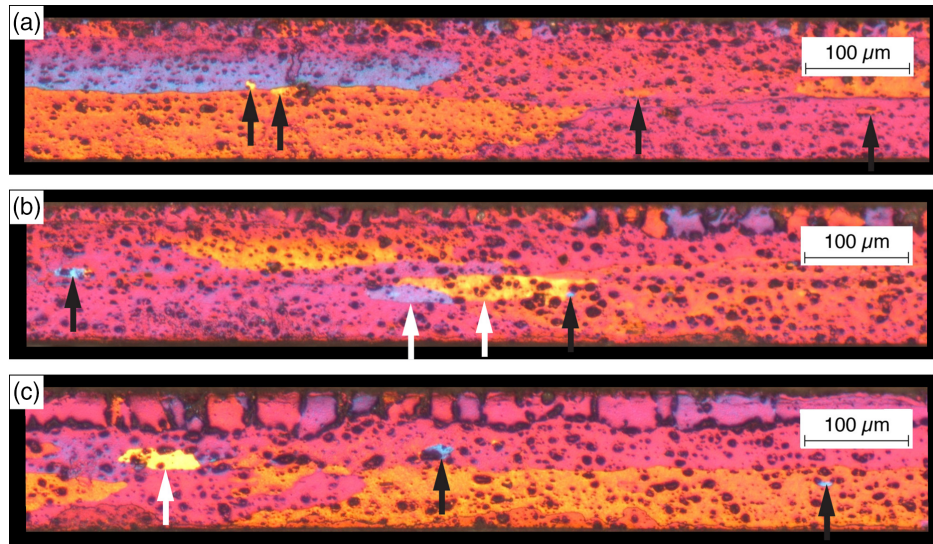


Figure 4. Cross-section-polarized LOM images showing the grain structure for a) the non-“brazed” zone, b) the transition region between the non-“brazed” and the “brazed” zones, and c) the fully “brazed” zone. Each grain is highlighted by a color, where different colors indicate contrasting crystal orientations of the grains. In the right side of (b) and in (c), the Al core material is affected by the braze clad in the braze simulation as large grains were formed in the solidified Al—Si alloy that grew into the core Al alloy. In addition, minute and small grains are present in the core material marked with black and white arrows, respectively.

3DXRD was conducted on strips of about 1 mm wide, 40 mm long, and 0.15 mm thick. One strip was cut out from the sample before the CAB simulation and one from the CAB simulated

coupon shown in Figure 3. Both strips had the long edge along the RD of the Al sheet. A result from the 3DXRD measurement of the sample before the CAB simulation is shown in **Figure 5**.

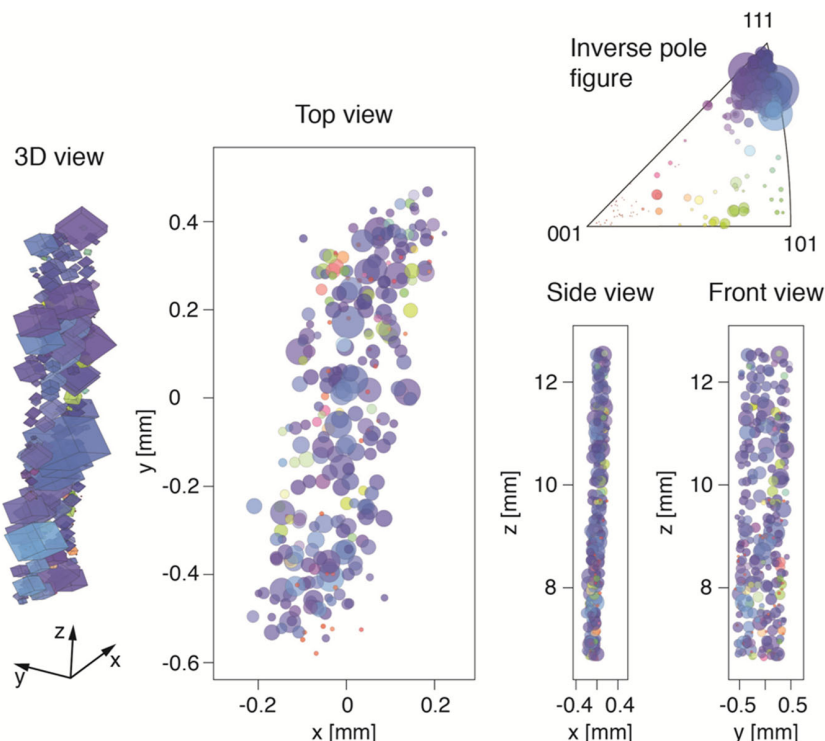


Figure 5. Maps showing the center-of-mass position of each grain in a braze clad Al sheet before braze simulation. Grain orientation is color coded based on the inverse pole figure. In the 3D view, the orientation of the cubes further indicates the grain orientations. The size of the cubes and the radius of the colored circles correspond to the relative size of the grains, which is estimated based on the intensity of the measured X-ray reflections.

The figure shows a 3D visualization of the center-of-mass positions and orientation of the Al grains as well as three orthogonal views of the center-of-mass positions (top view, side view, and front view) for the 1 mm-wide and 0.15 mm-thick strip over a 6 mm-long section of the sample. The size of the cubes in the 3D view and the radius of the colored circles in the top, side, and front views are proportional to the obtained diffraction spot intensities, which correspond roughly to the relative sizes of the probed grains.^[20] The orientations of the cubes in the 3D view, as well as their colors, and the color of the circles in the top-, side-, and front views indicate the grain orientations. Red, green, and blue represent the {001}, {101}, and {111} directions, respectively, as per the inverse pole figure of the ND. It can be seen that the dominating crystal direction of the grains in this untreated rolled Al sheet is {111}. There are also some grains with other orientations, mostly on one side of the strip, which is clearly seen on the right side of the front view in Figure 5 as greenish circles. These grains with orientations different from the {111} direction are on the edge that was cut using a shear cutter. Hence, it appears as though there is an effect on the crystal orientation of some of the grains that were fractured in the cutting process. In contrast, the other edges that were cut using

wire-cut electrical discharge machining (wire-EDM) do not show any deviation in grain orientation compared with the vast majority of the grains. Very few grains in the braze clad were detected by 3DXRD, indicating that they are too small to be detected. Consequently, only diffraction signals from the grains in the core materials were analyzed in the sample that had not been exposed to CAB simulations.

Figure 6 shows maps of center-of-mass positions of the sample after CAB simulation for a 1 mm wide strip cut along the RD of the coupon shown in Figure 3. The z-axis is along the transition region from the non-“brazed” zone at $z = 5$ mm, where the sample was kept below the melting point of the braze clad alloy, to the fully “brazed” zone at $z = 16$ mm, where the braze clad became molten in the CAB simulation. A comparison with Figure 5 indicates that there are many more grains detected; especially at $z > 7$ mm we can see many small grains with {001} orientation. However, around $z = 6$ mm there are no grains shown in the position, where one can expect there to be grains in the braze clad. As in the 3DXRD of the sample before the CAB simulation, as shown in Figure 5, the grains in the braze clad of the non-“brazed” zone are too small to be detected. Hence, the heat treatment up to temperatures below

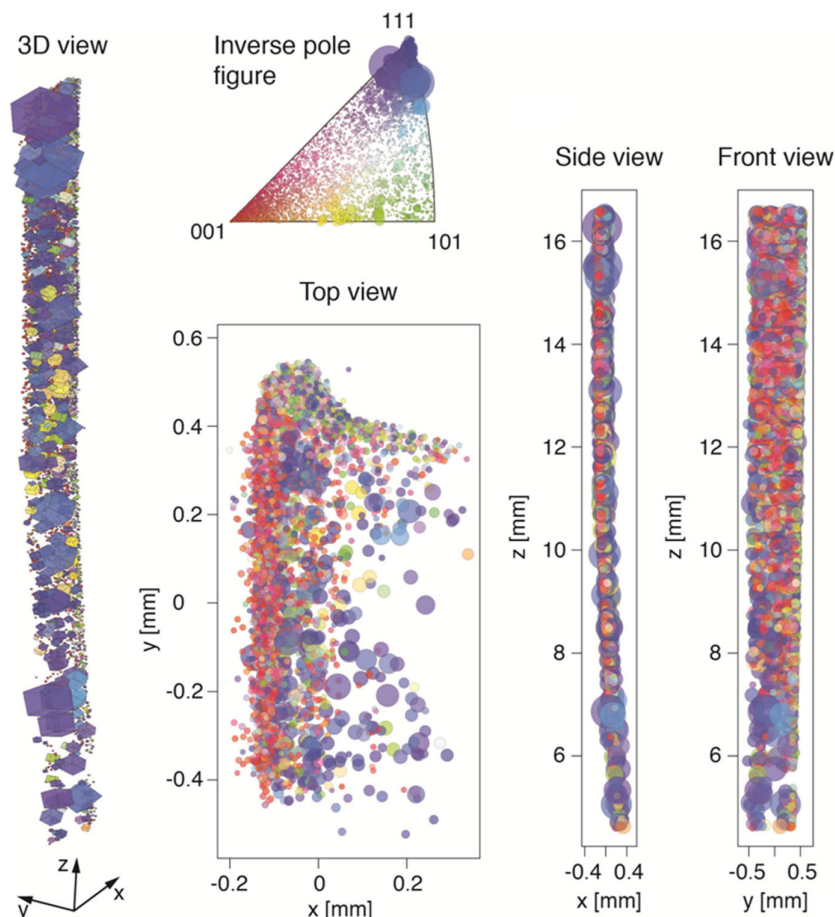


Figure 6. Maps showing the center-of-mass position of each grain in a braze clad Al sheet after braze simulation. Grain orientation is color coded based on the inverse pole figure. In the 3D view, the orientation of the cubes further indicates the grain orientations. The size of the cubes and the radius of the colored circles correspond to the relative size of the grains, which is estimated based on the intensity of the measured X-ray reflections.

the Al–Si alloy melting point does not seem to introduce significant grain growth in the braze clad. In contrast, grains that are large enough for detection can be observed in the side and front views for $z > 7$ mm, indicating that the solidification of the molten braze clad led to larger grains. The dominating crystal orientation of the new Al–Si alloy grains is the {001} direction, which is in contrast to the dominating {111} crystal direction in the core material. However, the inverse pole figure in Figure 6 shows a quite even distribution of crystal orientations for the new small grains. As in Figure 5, there are greenish circles visible on the right side in the side view in Figure 6. The number of greenish circles is significantly larger after the CAB simulation, which indicates that the surface after the shear cutting of the sample influences the grain orientation of small grains formed during or after the CAB simulation. It is also clear from the 3D view, top view, and front view that small-to-medium-sized grains with different orientations from the original {111} direction are introduced upon brazing also in the core material. This suggests that the process of 6% stretching of the sample before CAB simulation introduced additional energy to the material, so there is enough stored energy to activate a recrystallization process, at least locally, during heat treatment.

Figure 7 and 8 show two series of 3D images, indicating the distribution and orientation of grains in the two samples, where the relative grain size is within different ranges; the relative grain size is estimated based on the total intensity of the diffraction spots belonging to each grain^[20] normalized by the total intensity of the diffraction spots from the most intense grain. The comparison of the grains in the 0.1–0.2 range (i.e., the grains with a total intensity of 10%–20% of the most intense grain) shows that the distribution of grains in this size range is similar before and after a CAB simulation. A similar observation is made for the comparison in the 0.2–0.4 range, although it appears that the relative sizes of the grains in the CAB-simulated sample in Figure 8

are closer to the 0.2 limit. In the 0.4–1.0 range, in contrast, there are fewer large grains in the CAB-simulated sample compared with the sample before heat treatment. In addition, in both the 0.1–0.2 and 0.2–0.4 ranges, there are “yellow” grains in the CAB-simulated sample that are absent in the sample from before the CAB simulation. That the “yellow” grains are in the 0.1–0.4 range supports the suggestion of local recrystallization, probably induced by the additional energy from 6% stretching before the CAB simulation. Hence, it seems that the growth of the new grains has reduced the volume for many of the larger grains. Even so, the size of the largest grain in each sample is the same.

In the 0.02–0.05 and 0.05–0.1 ranges there are a lot of small grains in the sample exposed to the CAB simulation (Figure 8), whereas there are only a few grains in these size ranges before the CAB simulation (Figure 7). The majority of the small grains belong to the solidified Al–Si alloy material obtained after brazing and almost all of them are oriented along the {001} direction. However, a significant number of small grains with random orientation can be seen on the edge that was cut with a shear cutter before the CAB simulation. During CAB simulation, the molten braze clad flowed over the edge and because of gravity along the edge. Hence, the small grains with random orientation along the edge are solidified Al–Si material that wrap around the shear cut edge of the sample; the other three edges of the strip were cut using a wire-EDM after the CAB simulation. The small Al–Si grains with other orientations than {001} (green–yellow–pink–purple–turquoise–blue in Figure 5–8) are, thus, grown on core material grains with surfaces formed by the shear cutting process. This observation suggests that the crystal orientation of the Al–Si grains upon solidification of molten braze clad is influenced by the adjacent surfaces of the grains of the Al alloy core material at the braze clad/core material interface.

Further comparing the distribution of the {001} grains (red in Figure 5–8) in the 0.02–0.05 range and the 0.05–0.1 range shows

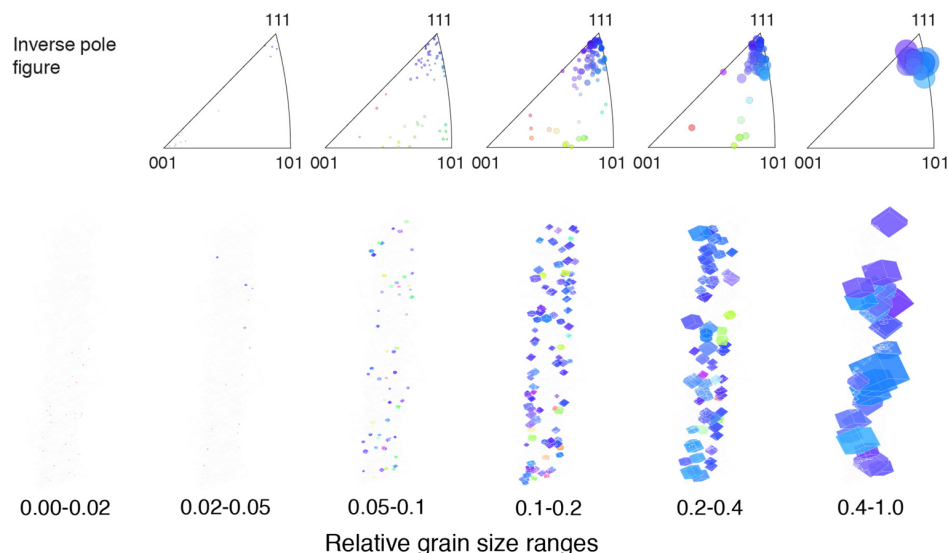


Figure 7. The 3D image of the braze clad Al sheet before braze simulation shown in Figure 5 where the obtained relative grain sizes are separated into different size ranges. Grain orientation is color coded based on the inverse pole figures and further indicated by the orientations of the cubes. The size of the cubes and the radius of the colored circles correspond to the relative size of the grains, which is estimated based on the intensity of the measured X-ray reflections.

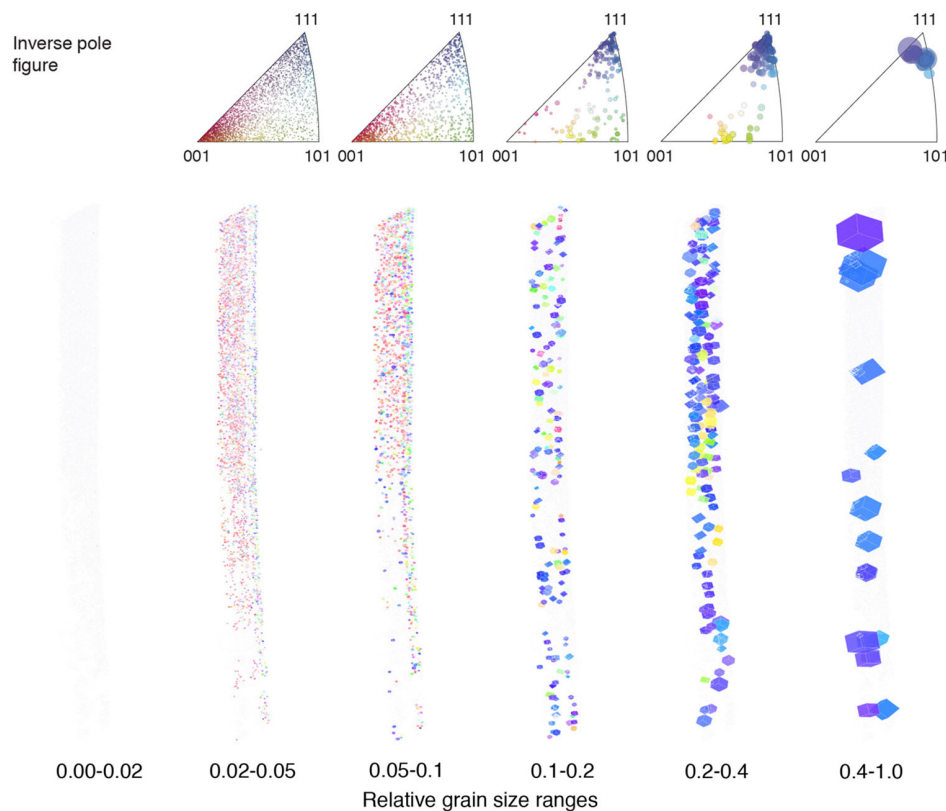


Figure 8. The 3D image of the braze clad Al sheet after braze simulation shown in Figure 6, where the obtained relative grain sizes are separated into different size ranges. Grain orientation is color coded based on the inverse pole figures and further indicated by the orientations of the cubes. The size of the cubes and the radius of the colored circles correspond to the relative size of the grains, which is estimated based on the intensity of the measured X-ray reflections.

that the transition region between the non-“brazed” zone and the fully “brazed” zone contains many small grains in the 0.02–0.05 range, but not in the 0.05–0.1 range. Hence, it is possible to distinguish three zones in the maps of center-of-mass position obtained from the 3DXRD: the non-“brazed” zone with very few {001} grains in both the 0.02–0.05 range and the 0.05–0.1 range; the transition region with many {001} grains in the 0.02–0.05 range but very few in the 0.05–0.1 range; the fully “brazed” zone with many {001} grains in both the 0.02–0.05 range and the 0.05–0.1 range.

Figure 9a,c show maps of center-of-mass positions of the sample before and after CAB simulation, respectively, where the color of the circles indicates the strain energy density (SED) in the grains. The SED is determined using the median lattice parameter for each sample as strain free reference and using the elastic constants from the study by Thomas.^[21] The top and front views in Figure 9a show that grains with SED near 0.1 MPa are mainly located in the vicinity of the right edge, i.e., the long edge in RD where the sample was cut with a shear cutter. After the CAB simulation, on the contrary, the few grains with SED near 0.1 MPa appear to be randomly distributed over the strip, as shown in Figure 9c. Hence, the provided heat in the CAB simulation led to recrystallization of the grains with SED near 0.1 MPa that originated from sample cutting. Figure 9b,d shows that it is mainly relatively large grains that have SED near

0.1 MPa. However, Figure 9d also shows that a large number of the small grains (relative grain sizes 0.02–0.05 and 0.05–0.1), which originate from the solidification of the molten Al–Si alloy, have SED around 0.06 MPa. This is especially evident in the region where there are a significant number of Al–Si grains that have grown into the core material, i.e., in the uppermost section in the 0.05–0.1 relative grain size range. The increased strain here could have been introduced during cooling.

3. Conclusion

Brazing of rolled Al sheets with braze clad involves a process of liquefying the Al–Si alloy in the braze clad followed by a solidification process. The present work has shown that synchrotron radiation-based 3DXRD can be an advantageous tool in the study of rolled Al alloy materials with braze clad for convenient brazing assembly of complex heat exchangers. Maps of the center-of-mass position of Al grains have been presented for two strips with Al–Si braze clad, obtained before and after CAB simulation. The results from the 3DXRD have shown that a significant number of grains are formed in the solidification process of the molten Al–Si alloy. These grains are oriented along the {001} direction, which is in contrast with the {111} orientation of the grains in the core Al material. It is also indicated

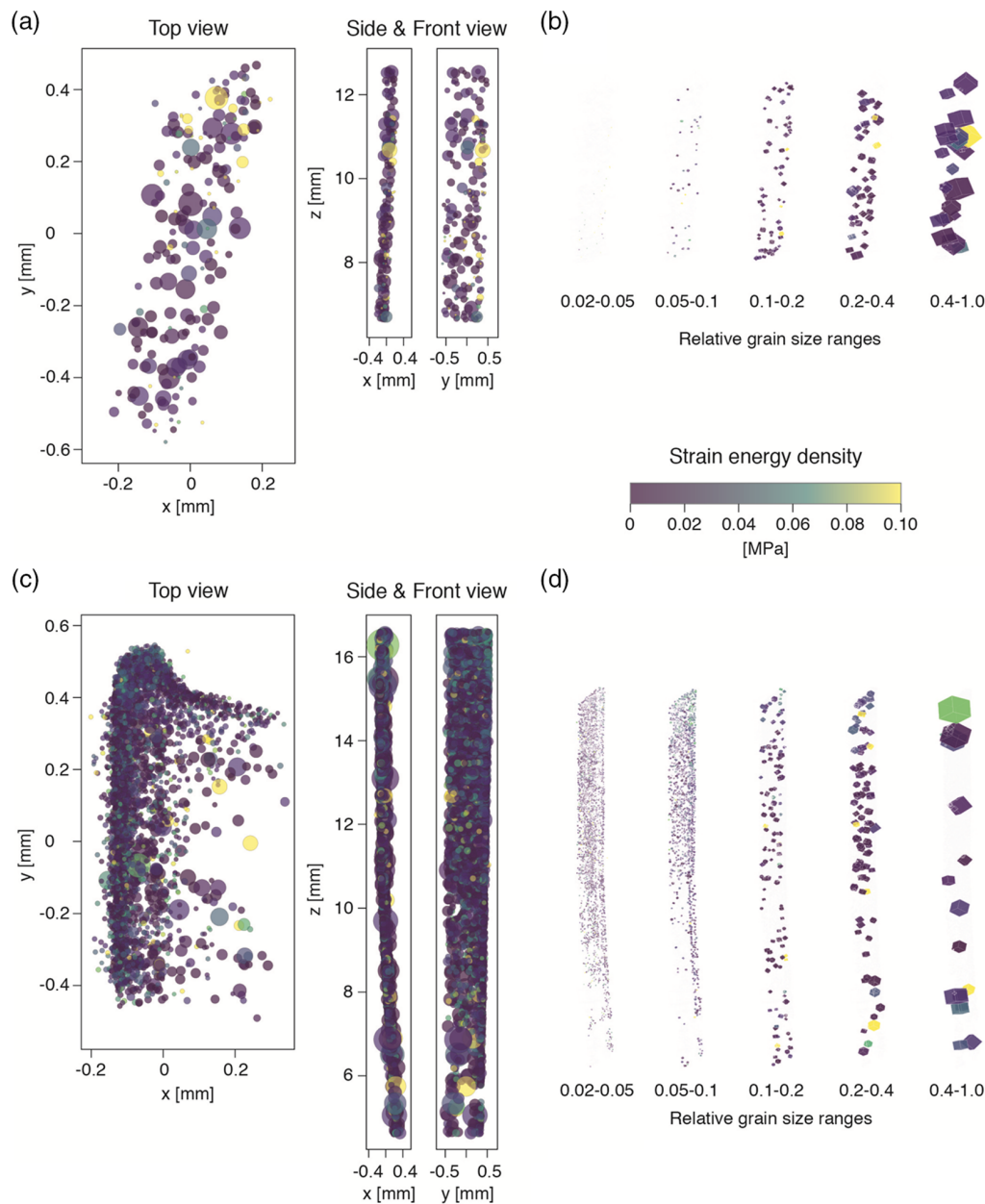


Figure 9. The SED as color-coded circles in maps and as color-coded cubes in 3D images. a,c) The center-of-mass position of each grain in a braze clad Al sheet before and after braze simulation, respectively. b,d) 3D images of the braze clad Al sheet before and after braze simulation, respectively. The obtained relative grain sizes are separated into different size ranges. The radius of the colored circles and the size of the cubes correspond to the relative size of the grains, which is estimated based on the intensity of the measured X-ray reflections.

that stretching the rolled Al sheet by 6% provides enough stored energy in the core material for local recrystallization to occur during brazing to form some grains with different orientations compared with the original grains oriented along the {111} direction. Further, the SED maps indicate that the braze cycle relaxes the material, although some grains retain a high strain. There are also indications in the 3DXRD data of larger grains that formed in the solidification process of the molten Al–Si alloy that had grown into the core material, as shown in the optical microscopy cross-section images. With the use of coloring from inverse pole

figures, it was possible to distinguish grains from the solidified Al–Si alloy, obtained after CAB simulation, from grains in the core Al alloy. It was also possible to distinguish the three zones: the non-“brazed” zone, the fully “brazed” zone, and the transition region between them. Hence, the obtained results show that further work using 3DXRD, in combination with other 3D imaging techniques, will provide valuable information regarding both wanted and unwanted processes in connection with brazing of mechanically formed Al alloy components in complex heat exchanger assemblies.

4. Experimental Section

Sample Preparation: The 128 μm -thick core material selected for this study was an Al alloy with 1.6% manganese (Mn), 1.5% zinc (Zn), 0.8% silicon (Si), 0.25% iron (Fe), and 0.1% zirconium (Zr). On one side of the rolled Al sheet, there was an 18 μm -thick layer of an Al braze clad alloy with 10% Si with an approximate melt interval between 577 and 590 °C. The material was produced in a commercial rolling mill, which included the hot and cold rolling processing steps and was subsequently annealed to be recrystallized and fully soft. This processing resulted in a material with a texture with preferred grain orientation. Before CAB simulation, the sample was stretched by 6% to simulate a sheet-forming process prior to brazing. Some recovery was expected to occur during heat treatment and some larger grains were expected to grow by consuming smaller grains. However, the core material should retain sufficient stored energy to drive a possible recrystallization process, especially at the interface between the core material and the braze clad. A $60 \times 20 \text{ mm}^2$ coupon was cut from the sample for convenient handling. The CAB simulation was conducted in a furnace with a nitrogen gas atmosphere at 590 °C. The heating ramp was 60 °C min^{-1} up to 500 °C, 25 °C min^{-1} between 500 and 575 °C, and 15 °C min^{-1} in the last 15 °C. Immediately after reaching 590 °C, the heating process was interrupted. A temperature gradient over the sample was obtained through cooling blocks attached to both ends of the coupon. Hence, at the furnace temperature of 590 °C, the braze clad in the middle part of the coupon was liquefied, whereas the braze clad at both ends remained solid. Between the non-“brazed” zone and the “brazed” zone, there was a transition region. After the CAB simulation, one-half of the coupon was cut by EDM (wire-cut type) into 1 mm-wide and 40 mm-long strips along the transition region from the non-“brazed” zone to the “brazed” zone.

Experimental Conditions: Optical microscopy was conducted using Zeiss Axio Imager M2m microscopes for the phase contrast images and the plane-polarized light images. The sample pieces were embedded in a polymer material and the cross-section cuts were along the RD and NDs of the samples. The exposed cross sections were polished using different abrasives at six steps. For grain structure images, the embedded sample pieces were anodized in a mixture of hydrogen fluoride acid, hydrogen tetrafluoroborate acid, ethanol, and water. The oxide growth of the exposed cross sections depends on the grain orientation, which will render as different shades of gray in plane-polarized light. With a one-fourth λ filter in the light path, the grains are shown with different colors.

The SMS P21.2 beamline at the synchrotron radiation facility PETRA III at DESY in Hamburg, Germany, was optimized for the combination of WAXS/SAXS with the possibility for 3D measurement by imaging techniques, such as 3DXRD, using broad- or narrow-bandwidth beams. The Al sample strips were illuminated by a monochromatic beam of 38.5 keV and diffraction images were obtained using a Varex XRD 4343CT area detector placed perpendicular to the beam direction and 856 mm from the sample. The pixel size of the detector was 150 μm and provided an angular resolution of 0.0028° in the 2θ diffraction angle, which corresponded to 0.0027 nm^{-1} resolution in reciprocal space. 3DXRD scans were made as the sample was rotated over 180° in 0.2° rotation intervals about a vertical axis with a 200 μm -high and 1.2 mm-wide beam. About 60 scans per sample were conducted with a vertical offset of the sample of 200 μm to cover the imaged length of the samples. The data were analyzed using the Fable software^[22] suite, following the theory described by Poulsen.^[23]

Acknowledgements

The authors acknowledge DESY (Hamburg, Germany), a member of the Helmholtz Association HGF, for the provision of experimental facilities. 3DXRD was conducted at beamline SMS P21.2 at PETRA III under proposal I-20190295 EC. The research was partly funded by Sweden's Innovation Agency (Vinnova) through grants 2018-03268 and 2019-05299. The data analysis was in part conducted with support from the QIM project at Lund University. The authors thank the metallurgical

department at Gränges Finspång AB for microscopy work and Linda Ahl and Anders Oskarsson at Gränges Finspång AB for valuable discussions.

Conflict of Interest

The authors declare no conflict of interest.

Data Availability Statement

Research data are not shared.

Keywords

3D X-ray diffraction, aluminum, controlled atmospheric brazing, grain orientations, inverse pole figures

Received: January 30, 2021

Revised: May 24, 2021

Published online: June 23, 2021

- [1] M. Nylén, U. Gustavsson, W. B. Hutchinson, A. Örtén, in *Aluminium Alloys, Proceedings of ICAA5, Materials Science Forum* (Eds: J. H. Driver, B. Dubost, F. Durand, R. Fougères, P. Guyot, P. Sainfort, M. Suéry), Vol. 217–222, Trans. Tech. Publication, Baech, Switzerland **1996**, pp. 1703–1708.
- [2] J. Lacaze, S. Tierce, M.-C. Lafont, Y. Thebault, N. Pébère, G. Mankowski, C. Blanc, H. Robidou, D. Vaumousse, D. Daloz, *Mater. Sci. Eng.: A* **2005**, 413–414, 317.
- [3] Å. Karlsson, in *INICAL '98 Proceedings of the International Conference on Aluminium* (Eds: D. H. Sastry, S. Subramanian, K. S. S. Murthy, K. P. Abraham), Vol. 1, The Aluminium Association of India, New Delhi, India **1998**, pp. 189–200.
- [4] D. J. Schmatz, *Weld. J. Res. Suppl.* **1983**, 62, 2675.
- [5] H. Suzuki, G. Itoh, K. Koyama, *J. Jpn. Inst. Light Met.* **1984**, 34, 708.
- [6] A. Örtén, K. Schölin, in *Vehicle Heat Exchanger and Transfer Design (SP-1175)*, SAE IC&E, Detroit MI **1996**, p. 960246.
- [7] M. Nylén, U. Gustavsson, W. B. Hutchinson, Å. Karlsson, in *Aluminium Alloys, Proceedings of ICAA7, Materials Science Forum* (Eds: E. A. Starke Jr, T. H. Sanders Jr, W. A. Cassada), Vol. 331–337, Trans. Tech. Publication, Baech, Switzerland **2000**, pp. 1737–1742.
- [8] R. Woods, *Liquid Film Migration during Aluminium Brazing*, SAE International **1997**, pp. 639–648.
- [9] A. Wittebrood, *PhD Thesis*, Technische Universiteit Delft, **2009**.
- [10] M. Kobayashi, Y. Takayama, H. Kato, *Mater. Trans.* **2004**, 45, 3247.
- [11] A.-L. Helbert, W. Wang, F. Brisset, T. Baudin, R. Penelle, *Adv. Eng. Mater.* **2012**, 14, 39.
- [12] D. Juul Jensen, E. M. Lauridsen, L. Margulies, H. F. Poulsen, S. Schmidt, H. O. Sørensen, G. B. M. Vaughan, *Mater. Today* **2006**, 9, 18.
- [13] Z. Hegedüs, T. Müller, J. Hektor, E. Larsson, T. Bäcker, S. Haas, A. L. C. Conceição, S. Gutschmidt, U. Lienert, *IOP Conf. Ser.: Mater. Sci. Eng.* **2019**, 580, 012032.
- [14] S. Schmidt, U. L. Olsen, H. F. Poulsen, H. O. Sørensen, E. M. Lauridsen, L. Margulies, C. Maurice, D. Juul Jensen, *Scr. Mater.* **2008**, 59, 491.
- [15] L. Renversade, A. Borbély, *J. Appl. Cryst.* **2017**, 50, 1144.
- [16] C. M. Hefferan, J. Lind, S. F. Li, U. Lienert, A. D. Rollett, R. M. Suter, *Acta Mater.* **2012**, 60, 4311.

- [17] N. Iqbal, N. H. van Dijk, S. E. Offerman, N. Geerlofs, M. P. Moret, L. Katgerman, G. J. Kearley, *Mater. Sci. Eng.: A* **2006**, 416, 18.
- [18] M. Faraji, J. P. Wright, L. Katgerman, *Mater. Lett.* **2010**, 64, 1016.
- [19] E. Nes, in *Encyclopedia of Materials: Science and Technology* (Eds: K. H. J. Buschow, R. W. Cahn, M. C. Flemings, B. Ilscher, E. J. Kramer, S. Mahajan, P. Veyssi re), Elsevier Ltd **2001**.
- [20] J. Als-Nielsen, D. McMorrow, *Elements of Modern X-Ray Physics*, 2nd ed., John Wiley & Sons, Inc., Chichester, West Sussex **2011**.
- [21] J. F. Thomas Jr, *Phys. Rev.* **1968**, 175, 955.
- [22] J. P. Wright, <https://github.com/FABLE-3DXRD/> (accessed: April, 2021).
- [23] H. F. Poulsen, *Three-Dimensional X-Ray Diffraction Microscopy: Mapping Polycrystals and Their Dynamics*, Springer Tracts in Modern Physics Vol. 205, Springer-Verlag, Berlin Heidelberg **2004**.